JVI Journals.ASM.org

Portal-Large Terminase Interactions of the Bacteriophage T4 DNA Packaging Machine Implicate a Molecular Lever Mechanism for Coupling ATPase to DNA Translocation

Shylaja Hegde,* Victor Padilla-Sanchez, Bonnie Draper, and Venigalla B. Rao

Department of Biology, The Catholic University of America, Washington, DC, USA

DNA packaging by double-stranded DNA bacteriophages and herpesviruses is driven by a powerful molecular machine assembled at the portal vertex of the empty prohead. The phage T4 packaging machine consists of three components: dodecameric portal (gp20), pentameric large terminase motor (gp17), and 11- or 12-meric small terminase (gp16). These components dynamically interact and orchestrate a complex series of reactions to produce a DNA-filled head containing one viral genome per head. Here, we analyzed the interactions between the portal and motor proteins using a direct binding assay, mutagenesis, and structural analyses. Our results show that a portal binding site is located in the ATP hydrolysis-controlling subdomain II of gp17. Mutations at key residues of this site lead to temperature-sensitive or null phenotypes. A conserved helix-turn-helix (HLH) that is part of this site interacts with the portal. A recombinant HLH peptide competes with gp17 for portal binding and blocks DNA translocation. The helices apparently provide specificity to capture the cognate prohead, whereas the loop residues communicate the portal interaction to the ATPase center. These observations lead to a hypothesis in which a unique HLH-portal interaction in the symmetrically mismatched complex acts as a lever to position the arginine finger and trigger ATP hydrolysis. Transiently connecting the critical parts of the motor; subdomain I (ATP binding), subdomain II (controlling ATP hydrolysis), and C-domain (DNA movement), the portal-motor interactions might ensure tight coupling between ATP hydrolysis and DNA translocation.

Tailed bacteriophages and herpesviruses use powerful ATP-driven machines to package their genomes into preformed capsid shells (36). They generate forces greater than 60 pN, ~20 times that of myosin motor, in order to compact a highly negatively charged, relatively rigid double-stranded DNA (dsDNA) to near-crystalline density (~500 μg/ml) (22, 39). The phage T4 employs one of the fastest and most powerful packaging machines reported to date. Packaging at a rate of up to ~2,000 bp/s, the T4 machine is estimated to generate twice the power (~5,000 kW/m^3) of an automobile engine (12, 36).

The T4 packaging machine consists of three components (Fig. 1): (i) an empty prohead containing a dodecameric portal protein, gp20 (25, 38); (ii) a pentameric large terminase motor protein, gp17 (5, 24, 42); and (iii) an 11- or 12-mer small terminase regulatory protein, gp16 (2, 24, 35). The cone-shaped portal links the head to the motor and DNA, with its wider end inside the capsid and the narrower end protruding outside. It has a central channel with a diameter of ~35 Å, through which DNA is threaded into the capsid. The portal works in conjunction with the motor, but its exact role is unclear. Various models such as the portal acting as a valve, DNA cruncher, or packaging sensor have been proposed (8, 9, 10, 38, 43).

Five molecules of gp17 assemble on the portal into a packaging motor (Fig. 1). gp17 consists of an N-terminal ATPase domain that provides energy for translocation and a C-terminal nuclease/translocase domain (1, 3, 19). The ATPase domain has a classic RecA type nucleotide-binding Rossmann fold, a six-stranded parallel β-sheet that is found in numerous ATPase motors (42). The nuclease/translocation domain has an RNase H fold found in RNase Hs, resolvases, and integrases and contains two DNA grooves—one for endonucleolytic cleavage to generate ends of packaged DNA and a second for translocation. The domains are connected by a flexible hinge, which facilitates interdomain interactions and domain movements. Powered by ATP hydrolysis, gp17 is proposed to alternate between relaxed and tensed conformational states, causing DNA movement in a piston-like fashion. Firing of all five motor subunits leads to translocation of about 10 bp (one helical turn) of DNA into the capsid (41).

The gp16 small terminase regulates the functions of the packaging motor (2, 14, 24). It has two long central helices that form an antiparallel coiled coil. Intersubunit interactions through these helices lead to the assembly of a vase-shaped cylinder containing a 24-to 34-Å central channel. The stoichiometry of the small terminase oligomer varies: 11- or 12-mer in T4 (40), 8-mer in Sf6 (47), 9- or 10-mer in SF6 (6), and 9- or 10-mer in P22 (30, 37). The small terminase recognizes the viral genome and interacts with gp17 to form a holo-terminase complex, which cleaves the concatemeric DNA. The end is then inserted into the portal channel, and gp16 stimulates gp17's ATPase activity to jump-start DNA packaging (24, 40).

The dynamic interactions among the packaging components are central to viral DNA translocation, but the sites of interaction and the mechanisms of regulation are poorly understood. For

Received 22 December 2011 **Accepted** 7 February 2012

Published ahead of print 15 February 2012

Address correspondence to Venigalla B. Rao, rao@cua.edu.

* Present address: Department of Vision Sciences, University of Alabama, Birmingham, Alabama, USA.

Supplemental material for this article may be found at http://jvi.asm.org/.

doi:10.1128/JVI.07197-11

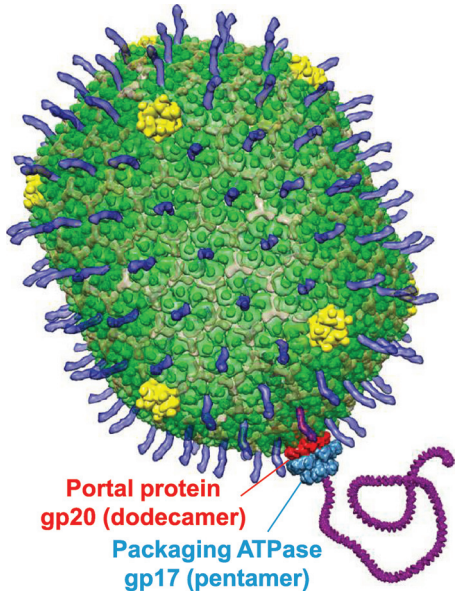

FIG 1 Structural model of the bacteriophage T4 DNA packaging machine. The model was constructed using the cryo-EM structure of prohead-bound gp17 (Electron Microscopy Database [EMDB] identification [ID] no. 1573). The dodecameric portal protein gp20 (red) and the pentameric packaging ATPase gp17 (light blue) translocate DNA (purple) into the T4 capsid. The major capsid protein gp23* is shown in green. gp24* vertices are shown in yellow, Soc (Protein Data Bank [PDB] no. 3IG9) is shown as translucent, and Hoc (the highly antigenic outer capsid protein; PDB no. 3SHS) is shown in blue.

instance, gp17 is a monomer in solution. It then assembles into a pentameric packaging motor on the portal, and after the head is filled, it dissociates and reconfigures into a DNA cutting complex of unknown stoichiometry (36). We have recently mapped some of the determinants involved in the small terminase and large terminase interactions, which show distinct specificities even among the T4 family terminases (13), as was observed in lambdoid phages (11). On the other hand, very little is known about the assembly of the motor on the portal and how the portal-motor interactions control DNA translocation. In phages λ and T3, genetic studies indicated that the last 6 to 10 C-terminal residues of large terminase might be involved in portal interaction (28, 29, 45, 46). However, in T4, two sites—one in the central region and another near, but not at the extreme, C terminus of gp17—were implicated (25, 26). Although binding of phage SPP1 large terminase to its portal has been demonstrated, the sites involved in portal interactions are unknown (32).

Here, using a series of biochemical, mutational, and structural analyses, we show that the central region of gp17 containing a helix-loop-helix (HLH) motif binds to the portal. Conservative substitutions at key residues of this motif lead to temperature-sensitive (*ts*) or null phenotypes, and recombinant peptides corresponding to HLH sequence block DNA translocation. The helices within the HLH motif provide specificity to bind to its cognate portal, whereas the loop region might be involved in triggering ATP hydrolysis. The HLH motif is part of ATPase subdomain II, the transmission domain that is responsible for coupling of ATP hydrolysis to DNA translocation. These observations lead to a molecular lever mechanism in which a unique interaction between the portal subunits and the HLH motif positions the arginine finger, triggering ATP hydrolysis and DNA translocation. The portal-motor symmetry mismatch allows this unique interaction to "travel" around the motor ring as the DNA is handed over from one motor subunit to the next.

MATERIALS AND METHODS

Bacteria, phage, and plasmids. *Escherichia coli* XL10 Gold-ultra competent cells (Stratagene, La Jolla, CA) were used for initial transformation of recombinant plasmids and for long-term maintenance. The plasmids were transformed into *E. coli* BL21(DE3)/pLys-S for expression of recombinant proteins. *E. coli* (mutant lacking the *sup* gene) was used for making infected extracts of T4 amber mutants used for prohead preparation. *E. coli* B40 (sup^1) was used for preparation of *17am18amrII* and other amber mutant stocks. *E. coli* strains containing the tRNA suppressor plasmids for Gly, Ala, Cys, Glu, Gln, Lys, Arg, Pro, His, Tyr, and Phe were used for construction of *F329am* and *F559am* mutants and their suppression analysis. The phage T4 *17F329am* and *17F559am* mutants were constructed as part of this study, and the *17K166am* and *17H436am* mutants were constructed previously (21). The plasmid vector pET28-b was used to construct the green fluorescent protein (gfp)-expressing gfp-gp17 and Soc-HLH fusion clones. pET15-b was used for combinatorial mutagenesis of portal binding sites I and II.

Construction of recombinant plasmids. PCR-directed splicing by overlap extension (SOE) (17) was used to clone the gfp gene (44) into the NheI site of pET28-b vector. The gfp gene was amplified using appropriate primers with a NheI restriction site incorporated at the 5′ ends and a gfp-reporter vector as the template. The recombinant gfp-expresssing plasmid (gfp-gp17) was purified, and full-length wild-type (WT) gp17 was inserted into the BamHI and XhoI restriction sites downstream of the gfp gene. The primers were designed such that insertion produced the gfp-gp17 fusion protein with a hexahistidine tag at the N terminus. Using this construct as a template, the gfp-gp17GSS-AAA mutant was constructed using appropriate mutant primers. All Soc-HLH clones were constructed by fusing the HLH sequences to the 3′ end of RB69-Soc sequence (phage RB69 is a close relative of T4) and amplified. The DNA was inserted into the NheI and XhoI sites such that the sequence was fused in-frame with the histidine tag at the N terminus. The sequence of all the clones was confirmed by DNA sequencing (Davis Sequencing, Inc., Davis, CA).

Mutagenesis. (i) Construction of the *17amF329* and *17amF559* mutants. To construct the *17amF329* and *17amF559* mutants, the amber mutations were first introduced into *g17* DNA by the SOE strategy (17). The DNA was cloned into the pET15-b vector, and the cells carrying the recombinant plasmid were spotted on *E. coli*-Phe suppressor plates. The cells were then infected with the *17amK166* (*F329am*) or *17amH436* (*F559am*) mutant by spotting the phage at the same spot. The progeny plaques were plated on *E. coli*-Phe suppressor, and individual plaques were screened for the presence of amber mutation on *E. coli* P301 (mutant lacking the *sup* gene). Since neither the *K166am* nor *H436am* mutant is suppressed by *E. coli*-Phe, all of the amber mutant plaques selected in this way should have the desired amber mutation at F329 or F559. Two independent plaques for each mutant were sequenced to confirm the presence of the correct amber mutation. The mutants were then tested on the 13 amber suppressors mentioned above to determine the phenotypes of various amino acid substitutions at each site (15).

(ii) Combinatorial mutagenesis. Combinatorial libraries were constructed at residues DD330 to 331 (DD330-331) and DY561 to 562 (DY561-562) using mutant primers having random nucleotides incorporated at the positions corresponding to these amino acids. The libraries were transformed into *E. coli* XL-10 Gold cells, and individual transformants were screened by recombinational marker rescue using either the *F329am* mutant (DD330-331 library) or the *F559am* mutant (DY561-562 library). The phenotype for each mutant was scored as functional (forms plaques), null (forms no plaques), *sp* (forms small plaques at 37°C), or *ts* (forms no plaques at 42°C). A WT *g17*-containing recombinant clone was

used as a positive control, and the vector alone was used as the negative control. Several hundred clones were screened to ensure that most, if not all, possible combinations were tested.

Isolation of second site suppressors. The *ts* (D331Q) mutation present on the plasmid was transferred into the T4 genome by recombinational marker rescue using *17amF329* mutant phage. After plaque purification, *E. coli* P301 cells were infected with the *17tsD331Q* phage at 42°C to 46°C, and the progeny phages were plated on *E. coli* P301 at 45°C. Two types of plaques were seen. DNA sequencing showed that the normal-size plaques are true revertants, changing Q to D, whereas the slightly smaller plaques have a second site mutation while retaining the original D331Q mutation. The phenotype of the latter was further confirmed by testing their plaque-forming abilities at different temperatures.

Purification of gfp-gp17 and Soc-HLH proteins. The *E. coli* BL21(DE3)/pLys-S cells containing the recombinant plasmid were induced with 1 mM isopropyl-β-D-thiogalactopyranoside (IPTG) at 30°C for 2.5 to 3 h. The cells were harvested by centrifugation and lysed using an Aminco French press (Thermo Fisher Scientific Inc., Waltham, MA). The cell lysates were centrifuged at 17,000 rpm for 30 min, and the supernatant was purified first by Histrap affinity column and then by Superdex 200 (GE Healthcare) according to the procedures described earlier (19). The purified protein was concentrated by Amicon ultra-15 centrifugal filters (Milipore, Temecula, CA) and stored at −70°C.

Purification of proheads. Proheads were isolated from *17am18amrII* mutant-infected cells by differential centrifugation and further purified by MonoQ ion-exchange chromatography according to the procedure described previously (20). Portal-minus proheads were prepared by treating the purified proheads with 0.1% SDS for 30 min, followed by sedimentation at 18,000 rpm for 45 min. Under these conditions, the portal is dissociated from the proheads and released into the supernatant, as confirmed by PAGE. The pellet containing portal-minus proheads was washed twice with prohead buffer (50 mM Tris-HCl [pH 7.4] containing 100 mM NaCl and 5 mM $MgCl_2$) and resuspended in the same buffer and stored at −70°C. The concentration of proheads was quantified by densitometry of the major capsid protein (gp23*; the star indicates the cleaved form) band following SDS-PAGE and Coomassie blue staining and comparing it with the gp23* band of a known amount of proheads or phage.

Prohead binding assay. Purified proheads (2×10^{11} particles) were incubated with gp17 at a gp17/gp20 ratio of 50:1 in 500 μl prohead buffer for 30 min at room temperature. The proheads were sedimented by centrifugation at 18,000 rpm for 45 min at 4°C. The pellet was washed twice with 1 ml prohead buffer and resuspended in 20 μl of the same buffer. The samples were electrophoresed by SDS-PAGE followed by staining with Coomassie blue. gp17 was quantified by ImageQuant software using the gp20 and gp23* bands in the same lane as internal standards.

DNA packaging inhibition assay. DNA packaging assays were done in a 20-μl reaction mixture containing 4×10^9 proheads, gp17 (1 μM), and 600 ng of phage lambda DNA in 65 mM Tris-HCl (pH 7.5), 5 mM $MgCl_2$, and 80 mM NaCl. To test the effect of Soc-HLH peptide on DNA packaging, the proheads were first saturated with excess RB69 Soc (10:1 ratio of Soc to Soc binding sites) added to the reaction mixture. In the control experiments, addition of the same amount of Soc showed no effect on DNA packaging. Soc-HLH peptide and gp17 were then added to the proheads at a peptide/gp17 ratio of 6:1, or as indicated in the figures, and incubated at 37°C for 15 min. ATP and the rest of the packaging components were added, and the reaction mixtures were incubated at 37°C for 45 min. DNase I was added to a final concentration of 0.5 μg/μl and incubated at 37°C for 30 min to degrade the unpackaged DNA. The reaction mixture was then treated with proteinase K cocktail (50 mM EDTA, 0.5 μg/μl proteinase K, 0.2% SDS) and incubated at 67°C for 30 min. The reaction mixture was separated by electrophoresis on an agarose gel (wt/vol), and the DNA was stained with Sybr green. The packaged DNA was quantified using the Gel DOC XR imaging system (Bio-Rad). The amount of DNA packaged in the absence of Soc-HLH peptide (positive control) was considered 100%, and the activities in the presence of various peptides were normalized to that of the positive control.

ATPase assay. Purified gp17 or mutants (1.5 μM) were incubated at 37°C for 15 min in the ATPase reaction buffer (50 mM Tris-HCl [pH 7.4] buffer containing 100 mM NaCl and 5 mM $MgCl_2$). To this, gp16 (8 μM) and ATP (1 mM cold ATP and 75 nM [γ-^{32}P]ATP; specific activity, 3,000 Ci [111 TBq]/mmol) were added, and the volume was adjusted to 20 μl. The reaction products were separated by polyethylenimine (PEI) thin-layer chromatography and quantified as described earlier (24).

Bioinformatics. Multiple sequence alignments of large terminases of T4 family phages were compiled using ClustalW (http://www.ebi.ac.uk/Tools/clustalw2/index.html) with default parameters. Structural analyses and images were created with PyMOL (http://pymol.sourceforge.net), and other images and the movie in the supplemental material were created with UCSF Chimera (http://www.cgl.ucsf.edu/chimera).

RESULTS

gp17 binds to proheads. We have developed a direct binding assay to analyze the interaction of gp17 with the prohead. In this assay, empty expanded proheads purified from *17am18amrII* phage-infected cells were incubated with gp17 and sedimented by high-speed centrifugation. Cosedimention of gp17 with proheads (Fig. 2A, lane 1; compare to control lane 3) indicated that gp17 binds to proheads. In parallel experiments, no significant binding was observed with a nonspecific protein such as bovine serum albumin (BSA) (lane 4).

Proteins with similar molecular masses, such as gp17 (70 kDa), gpAlt (70 kDa), gp17 K577 (C-terminally truncated [13]) (63 kDa), and gp20 (61 kDa), and the low copy number of gp17 compared to the major capsid protein made it difficult to analyze the gp17 binding parameters. Therefore, a modified gp17 was constructed by fusing the gfp gene to the N terminus of gp17, which increased the molecular mass of gp17 by 29 kDa (Fig. 2B) and the gfp-gp17 fusion protein was purified to near homogeneity (Fig. 2C). Functional studies showed that the gfp-gp17, like its WT counterpart, exists as a monomer in solution, as determined by size exclusion chromatography and shows very similar functional activities such as gp16-stimulated ATPase, nuclease, and DNA packaging (data not shown).

gfp-gp17 bound to the prohead as efficiently as the WT gp17, as shown by the appearance of a 104-kDa band in the sedimented proheads, which was clearly separated from the gpAlt and gp20 bands (Fig. 2D, lanes 3 to 5 [see arrow], compared to the control lane 2). Binding was specific because proheads incubated with gfp alone showed no binding (Fig. 2D, lane 6). Binding increased with increasing ratio of gfp-gp17 to proheads reaching a maximum at a ratio of 50:1 (lane 4). The copy number of bound gp17 per prohead quantified from independent experiments ($n = 14$) is about 5.

gp17 binds to gp20 portal. To test if gp17 binds to prohead through its interaction with the gp20 portal, portal-minus proheads were prepared (see Materials and Methods) and incubated with gfp-gp17, but no significant binding was observed (Fig. 3A, lane 4; compare to lane 2 showing gfp-gp17 binding to the WT proheads). Binding was also not detected when gp17 was incubated with mature phage T4 in which the portal binding sites are no longer exposed due to the assembly of neck and tail on the portal (lane 6).

A portal interaction site is located in the N-terminal domain of gp17. gp17 consists of two domains, an N-terminal ATPase domain (N360; amino acids [aa] 1 to 360) and a C-terminal nu-

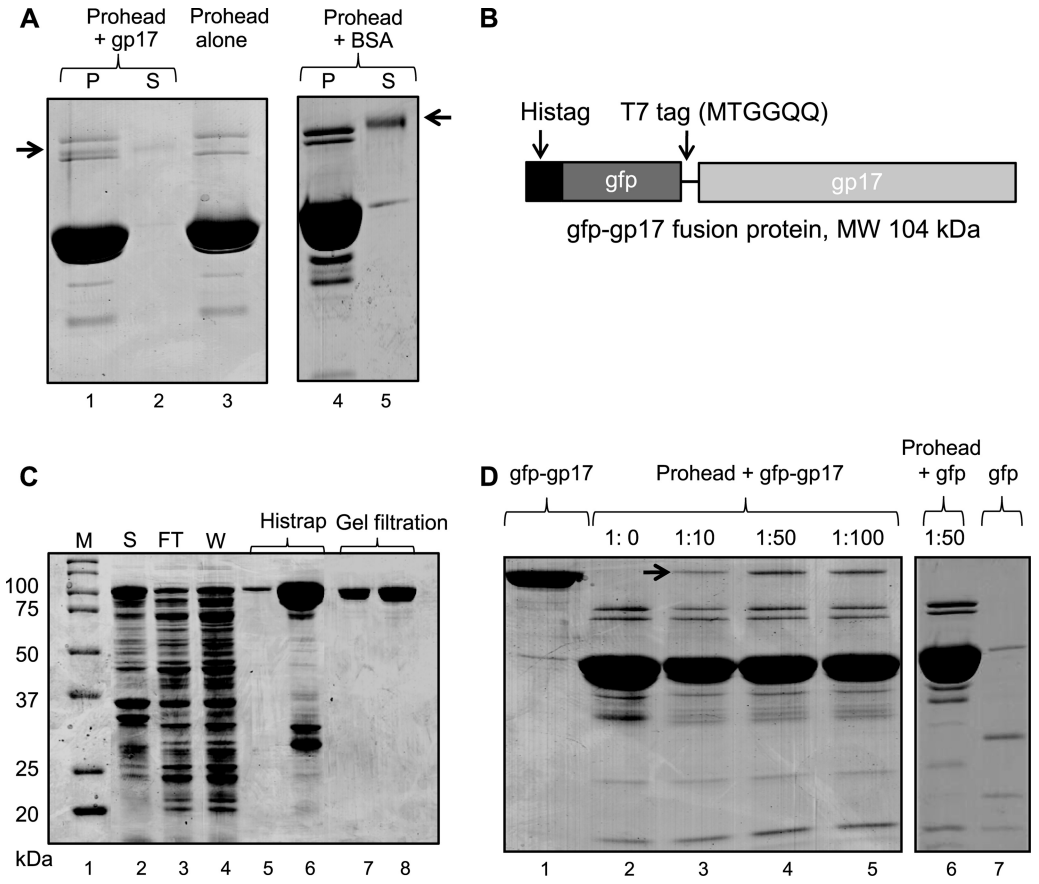

FIG 2 gp17 binds to prohead. Binding assays were performed according to the procedure described in Materials and Methods. (A) Proheads (30 nM; 2×10^{11} particles) were incubated either alone (lane 3) or with gp17-K577 (lane 1) or BSA (lane 4). Lanes 2 and 5 show unbound K577 and BSA, respectively, in the supernatant fraction. (B) Schematic of the gfp-gp17 fusion construct. The gfp sequence (44) was fused to the N terminus of gp17 with a T7 tag as a linker in between. (C) Overexpression and purification of gfp-gp17. The *E. coli* lysate (lane 2) was applied to the Histrap column. Lanes 3 and 4 show flowthrough and wash fractions, respectively. The gfp-gp17 fractions eluted with imidazole (lanes 5 and 6) were pooled together and applied to Superdex-200 size exclusion column. The peak gfp-gp17 fractions (lanes 7 and 8) were collected and used for binding assays. Molecular mass markers (M) are shown in lane 1. (D) Binding of gfp-gp17 to proheads. Proheads (2×10^{11}) were incubated with increasing ratios of gfp-gp17 to gp20 (lanes 2 to 5) or gfp at ratio of 1:50 to gp20. Lanes 1 and 7 show unbound gfp-gp17 and gfp, respectively.

clease/translocase domain (C360; aa 361 to 577) (19, 41). To identify which of these domains has the portal interaction site, prohead binding experiments were performed using purified domains. At a 100 mM NaCl concentration, both N360 and C360 bound to the proheads (Fig. 3B, lanes 1 and 3), but at a 300 mM NaCl concentration, N360 binding to proheads remained nearly the same (lane 2), whereas C360 binding was reduced (lane 4), suggesting that C360 binding might be nonspecific.

A portal binding site in the central region of gp17. Sequence alignments and genetic data suggested two potential portal interaction regions in gp17: LYNDEDIFDD (aa 323 to 331) (site 1) and FIDYADKDD (aa 559 to 567) (site II) (Fig. 4A) (25, 26). These residues are well conserved among the T4 family large terminases and contain clusters of acidic and hydrophobic residues similar to portal interaction sites proposed for phage λ (45, 46) and T3 (28, 29) terminases. The importance of these sites for gp17 function was determined by combinatorial mutagenesis. First, two amber mutants, one in each site, were constructed at residues F329 and F559. The amber mutations were transferred into phage T4 genome by recombinational rescue, and the effect of 13 different amino acid substitutions at each site was tested by plating the mutants on the respective *E. coli* suppressor strain. The results show that F329 is important for function as the *F329am* phage tolerated only a few conservative substitutions (Fig. 4B), whereas the *F559am* phage tolerated less conservative substitutions, including alanine and cysteine (Fig. 4C).

Two combinatorial mutant libraries were then constructed at the conserved residues D330 to D331 and D561 to Y562. Each mutation was transferred into T4 genome by recombinational exchange using the mutant phages *F329am* (D330-D331 library) or F559*am* (D561-Y562 library), and the phenotypes were scored as "functional" (lysis) or "null" (no lysis). Of the 780 DD330-331 mutants tested, only 6 (0.7%) exhibited a functional phenotype. DNA sequencing showed that all the mutants retained aspartic acid at least at one of the positions and a conservative substitution (glutamic acid, asparagine, or glutamine) or a neutral amino acid (alanine or cysteine) at the second position (Fig. 4B). On the other hand, ~47% of the D561-Y562 mutants are functional, with many containing nonconservative substitutions such as Pro561-Ala562 (Fig. 4C).

The DD functional mutants were tested for conditional lethality at 3 different temperatures: 25°C, 37°C, and 42°C. Of the six

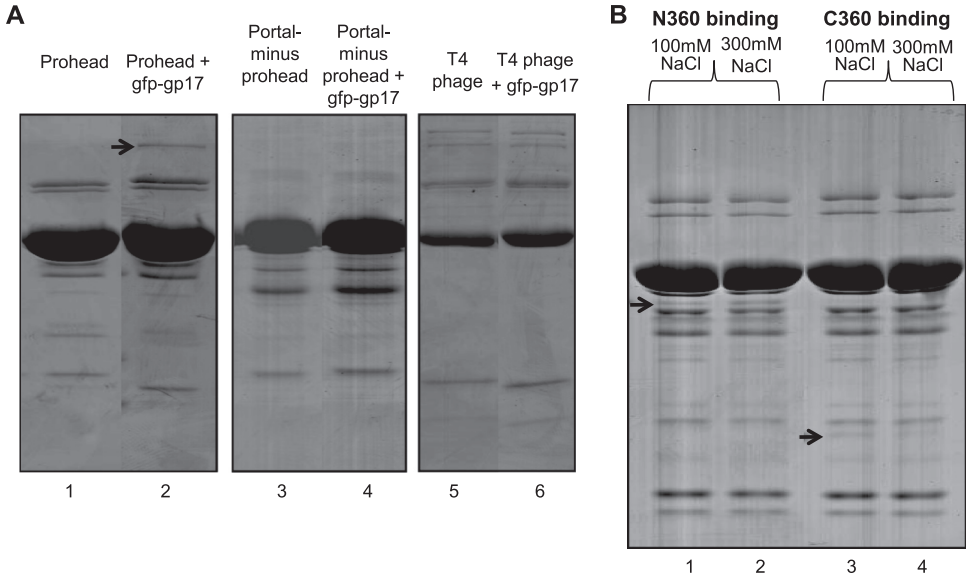

FIG 3 The N-domain of gp17 binds to proheads through its interaction with gp20 portal. (A) The binding assays were done under standard conditions using 2×10^{11} proheads (lanes 1 and 2), portal-minus proheads (lanes 3 and 4), or phage (lanes 5 and 6) and ± gfp-gp17 at a molar ratio of 1:50 (gp20 to gfp-gp17). The position of gfp-gp17 is indicated with an arrow. Note that the recovery of portal-minus proheads by centrifugation was less efficient than that of the WT proheads. (B) The N360 and C360 domains were purified according to the procedures described previously (19). The binding assays were done under standard conditions using 2×10^{11} proheads and a molar ratio of gp20 to N360/C360 of 1:50. The NaCl concentrations used were 100 mM and 300 mM. Arrows indicate the positions of N360 and C360 bands in the respective lanes.

mutants, one has the WT sequence and as expected displayed the functional phenotype at all temperatures. Three mutants exhibited a *ts* phenotype and did not form plaques at 42°C, and two exhibited a severe *ts* phenotype, forming no plaques at 42°C and only small to minute plaques at 37°C (Fig. 4D). These results demonstrate that even conservative substitutions at site I led to defects in gp17 function, with the D330 substitutions being the most severe.

A helix-loop-helix (HLH) motif is involved in portal interaction. To isolate second site suppressors, the *17ts* D331Q mutation was transferred into T4 genome by recombinational rescue using *17K166am* phage. The *ts* phage was then used for infections at 42°C to 46°C, and the progeny phages were plated at 45°C. Five suppressors were identified based on their smaller plaque size. (The normal-size plaques turned out to be true revertants.) Of these, four have a second site mutation changing isoleucine to methionine at residue 337, and the fifth also changed the same residue, but changed it into lysine (Fig. 4D). The I337 residue is part of a helix-loop-helix motif that is adjacent to the loop containing the original D331Q mutation (see below).

Evidence that the HLH motif interacts with gp20. Cryo-electron microscopy (cryo-EM) and X-ray structure analyses showed a pentameric packaging motor assembled at the portal vertex of the empty prohead (41). Consistent with our biochemical and genetic findings, fitting of the gp17 X-ray structure into the cryo-EM density showed that the N-terminal domain indeed interacts with the portal (Fig. 5A). Although the 32-Å resolution of the cryo-EM density does not allow for identification of the exact motor-portal interactions, it shows that the HLH region protruding from the otherwise flat N-domain surface would be the most likely point of contact (Fig. 5B).

To determine if the HLH motif binds to the portal, the sequence WQWSIQTINGSSLAQFRQEH (aa 333 to 352), corresponding to the HLH peptide, was fused to the N terminus of the RB69 small outer capsid protein, Soc (9 kDa) (Fig. 6A). Our recently determined atomic structure of Soc shows that its N terminus is unstructured and well exposed to the solvent (34). Three HLH peptide-Soc fusions were constructed: the first containing the WT peptide sequence (HLH-wt), a second with an F348A mutation that increased solubility, and a third containing a scrambled sequence, SAEQNIWTSQIGHLQWFRQS (HLH-scr). The recombinant proteins were overexpressed and purified.

If the HLH peptide interacts with the portal, it should compete with gp17 for portal interaction and interfere with the assembly of the packaging machine. Indeed, in numerous experiments, the Soc-HLH-wt peptide inhibited up to ~80% of the DNA packaging activity at a 6:1 molar ratio of peptide to gp17 (Fig. 6B, lane 4, and C). The HLH-F348A peptide which is more soluble than the HLH-wt peptide, also displayed the same level of inhibition of DNA packaging (lane 8). However, the HLH-scr peptide displayed no inhibition at the same or higher ratio (Fig. 6B, lane 6, and C). In control experiments, the peptides did not affect the intrinsic gp17 functions such as the gp16-stimulated ATPase activity, which does not require portal interaction (data not shown).

Direct binding of Soc-HLH peptides to the portal could not however be accurately quantified in the above experiments due to some background binding of Soc-HLH to capsid through Soc, even though the *17am.18am.rII*-expanded proheads should have full occupancy of Soc and excess RB69 Soc was added to saturate any unfilled sites (see Materials and Methods). (Note the presence of excess Soc did not affect the DNA packaging efficiency.) Therefore, another series of recombinants were constructed to demonstrate direct binding. The HLH peptides were fused to the C terminus of gfp, and the recombinant peptides were purified. The gfp-fused HLH-wt peptide, but not the HLH-scr peptide, bound to proheads, but no significant packaging inhibition was observed

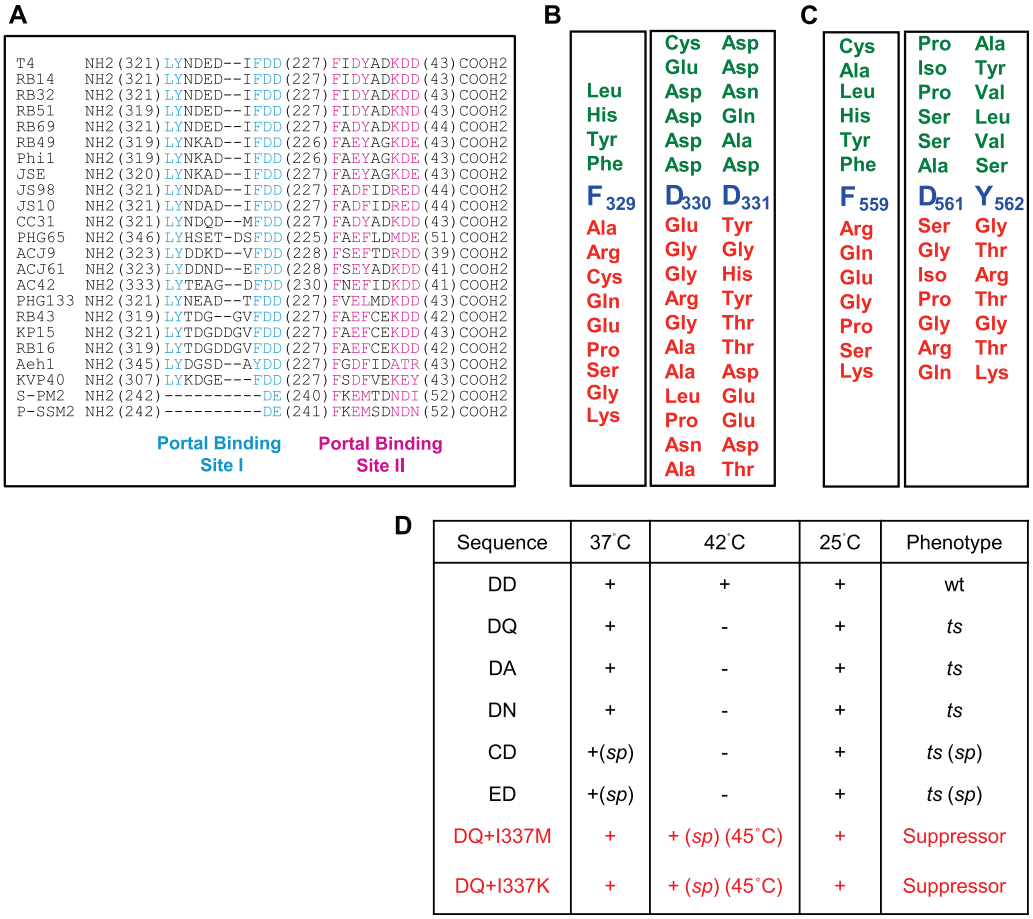

D

Sequence	37°C	42°C	25°C	Phenotype
DD	+	+	+	wt
DQ	+	-	+	*ts*
DA	+	-	+	*ts*
DN	+	-	+	*ts*
CD	+(*sp*)	-	+	*ts* (*sp*)
ED	+(*sp*)	-	+	*ts* (*sp*)
DQ+I337M	+	+ (*sp*) (45°C)	+	Suppressor
DQ+I337K	+	+ (*sp*) (45°C)	+	Suppressor

FIG 4 Characterization of a portal binding site in the N-terminal domain of gp17. (A) Sequence alignment of T4 family phage terminases by ClustalW. The numbers in parentheses represent the amino acids that are not shown in the alignment. The conserved residues (>90%) from the putative portal binding sites I and II are highlighted in cyan and magenta, respectively. All sequences were obtained from GenBank. The accession numbers are as follows: T4, P17312; RB14, YP_002854500; RB32, YP_803107; RB51, YP_002854122; RB69, NP 861869; RB49, NP 891724; Phi1, YP_001469498; JSE, YP_002922229; JS98, YP_001595293; JS10, YP_002922510; CC31, YP_004010027; PHG65, YP_004300928; ACJ9, YP_004010314; ACJ61, YP_004009792; AC42, YP_004009538; PHG133, YP_004300751; RB43, YP_238880; KP15, YP_003580049; RB16, YP_003858506; Aeh1, NP 944105; KVP40, NP 899601; S-PM2, YP_195134; and P-SSM2, YP_214360.1. (B) Mutational analysis of conserved residues F329 and DD330-331 of portal binding site I. The importance of F329 for function was analyzed by a suppressor-based genetic approach, and that of DD330-331 was analyzed by a combinatorial approach. Functional substitutions that produced plaques are shown above (green) and null substitutions are shown below (red) the native sequence (blue). (C) Mutational analysis of conserved residues F559 and DY561-562 of portal binding site II. The importance of F559 for function was analyzed by a suppressor-based genetic approach, and that of DY561-562 was analyzed by a combinatorial approach. Coloring is as in panel B. See Materials and Methods for details on the mutagenesis and screening procedures. (D) Functional mutants in portal binding site I were tested for plaque-forming ability at three temperatures: 25°C, 37°C, and 42°C. Each mutant was scored as wt (normal-size plaques), *ts* (no plaques), or *sp* (small or minute plaques). "+" means normal plaques, and "−" means no plaques. The phenotypic features of the second site mutant (D331Q) are shown in red.

with the gfp-fused HLH peptides. This might be because the bulky gfp interfered with a step following initial interaction that is necessary for competition with gp17.

From the above series of experiments, we conclude that the HLH-wt peptide binds to the portal and interferes with the assembly of the functional packaging motor.

Dissection of the functional roles of the HLH motif. Sequence alignments and secondary structure predictions suggest that the HLH motif is structurally conserved among the T4 family phages (Fig. 7A). However, sequence variations are observed in the helices, whereas the loop residues are relatively well conserved. We hypothesize that the HLH motif consists of constant and variable regions. The constant loop residues are likely involved in the functional aspects of the packaging machine—for example, regulation of ATP hydrolysis. On the other hand, the helix residues might serve as specificity determinants, allowing efficient interaction between gp20 (portal) and gp17 (motor) belonging to the same phage. Such selectivity, also seen in the large and small terminase interactions (13), might be essential to maintain the fidelity of packaging machine assembly when the same *E. coli* cell is infected by more than one T4 family phage.

To test this hypothesis, three swap mutants were constructed. In each, the residues of either the helices or the loop of one phage were swapped with those of another phage from T4 family. All of the swaps were constructed as fusions to Soc. In mutants 1 and 2, the variant residues of phages RB43 and RB49 in helix 1 and helix 2 were swapped with T4 (Fig. 7B). In mutant 3, the loop sequence of T4 was swapped with that of phage S-PM2 (Fig. 7B). In addition, the F348A mutation was introduced into all constructs to enhance the solubility of the HLH peptides.

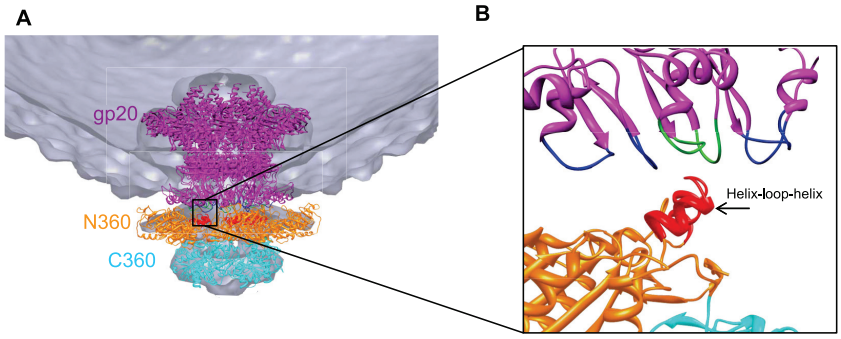

FIG 5 The HLH motif of gp17 contacts the portal protein. (A) Fitting of the gp17 pentamer (PDB ID no. 3EZK) and the gp20 dodecamer (pseudoatomic model; V. Padilla-Sanchez and V. B. Rao, unpublished data) into the cryo-EM density of the motor-bound procapsid (32-Å resolution; EMDB ID no. 1572) shows that the N-terminal ATPase domain of gp17 (N360; orange) is oriented toward the portal (violet). (B) A close-up view of the boxed region in panel A shows that HLH motif of gp17 (red) is the point of contact with the portal protein. Loops of portal subunits are alternately colored blue and green.

The recombinant swap mutant peptides were purified and tested for their effect on DNA packaging. The results indicate that the helix swap mutants did not show any packaging inhibition (Fig. 7C, lanes 5 and 8; and D), whereas the loop mutant exhibited ~60% inhibition (Fig. 7C, lane 11, and D). This suggests that the variant RB43 or RB49 HLH motifs could not effectively compete with the WT T4 gp17 for interaction with its cognate portal. On the other hand, the loop mutant where the helix sequences are intact could compete with T4 gp17 for portal binding and interfere with the DNA packaging activity.

The loop of the HLH motif regulates ATP hydrolysis. To further analyze the role of the HLH loop, mutations were introduced by changing the loop residues GSS to AAA in the background of full-length gfp-gp17, and the recombinant protein was purified (Fig. 8A). The gfp-gp17 loop mutant bound to proheads as well as the WT gp17 (Fig. 8B), but it showed severely reduced gp16-stimulated ATPase activity, even when 4-fold more mutant protein was added (Fig. 8C, compare lanes 5 to 7 with lane 4). The GSS-AAA mutant displayed no DNA packing activity (Fig. 8D, lanes 3 to 6), but it competed for gp17 binding to the portal and inhibited ~95% of the WT gp17's DNA packaging activity (Fig. 8E, lane 6).

DISCUSSION

Our recent biochemical and structural analyses defined the catalytic motifs of the phage T4 DNA packaging machine, in particular those involved in energy production and generation of genomic termini (15, 20, 35, 36). An electrostatic force-driven translocation mechanism has been proposed (41), but the dynamic aspects of the mechanism such as the assembly and disassembly of various complexes and how they are mechanistically linked to DNA movement, remain poorly understood. Unlike the catalytic signatures that are conserved in numerous molecular motors, the interaction motifs are unique to each phage and even distinct among members of the same phage family. Such selectivity might impart specificity to packaging partners such that the right genome is inserted into the right capsid in mixed infections that frequently

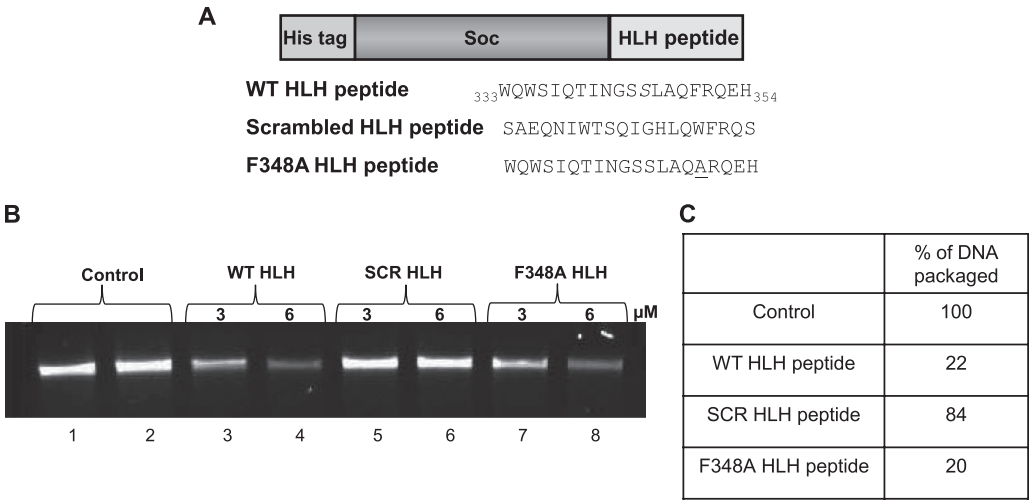

FIG 6 An HLH peptide binds to the portal protein. (A) Schematic of the recombinant HLH peptide constructs. The WT and scrambled sequences of the HLH motif (as shown) are fused in-frame to the C terminus of RB69 Soc (34). (B) Inhibition of *in vitro* DNA packaging by HLH peptide. *In vitro* DNA packaging assays were performed as described in Materials and Methods (20). Proheads (4×10^9 particles) were first incubated with HLH peptide (WT, scrambled [SCR], or F348A) for 15 min, after which the rest of the packaging components were added. The agarose gel shows DNA packaging with 1 μM gp17 alone (control lanes 1 and 2) or in the presence of WT peptide (lanes 3 and 4), scrambled peptide (lanes 5 and 6), or F348A peptide (lanes 7 and 8). (C) Relative amounts of DNA packaged by reactions in panel B.

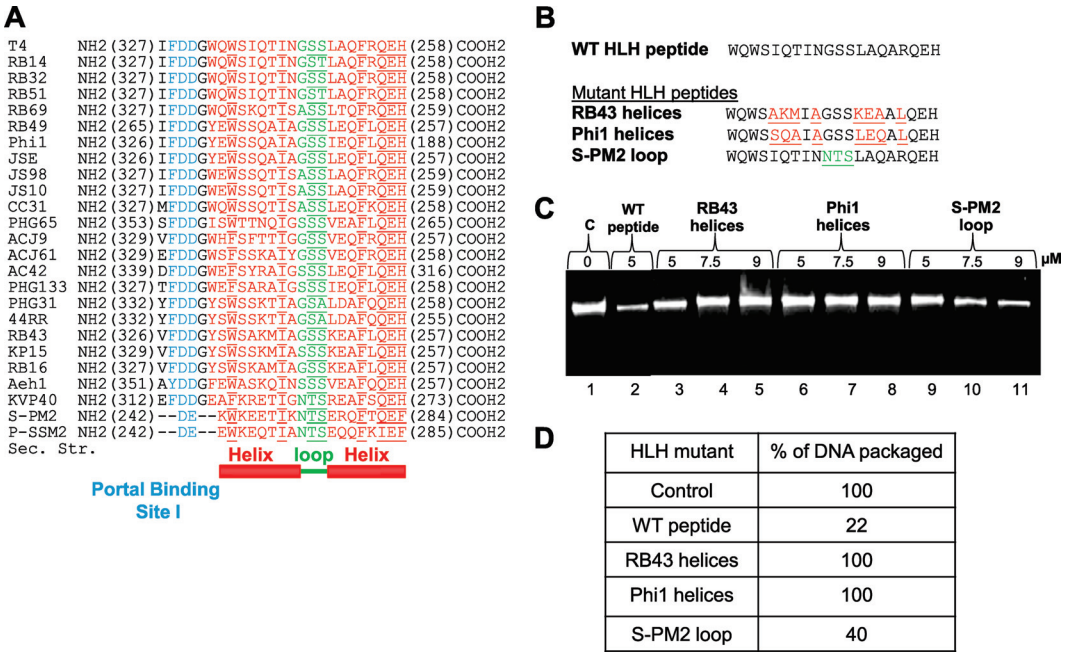

HLH mutant	% of DNA packaged
Control	100
WT peptide	22
RB43 helices	100
Phi1 helices	100
S-PM2 loop	40

FIG 7 Dissecting the functional roles of residues in the helix and loop regions of the HLH motif. (A) Sequence alignment of the HLH motifs of T4 family large terminases. The helices are shown in red and the loop in green. Highly conserved amino acids (>90% identity) are underlined. The portal binding site I (Fig. 4) is highlighted in cyan. (B) Sequences of HLH swap mutants. The T4 (WT) sequence is shown in black. Mutations introduced in the helix region (red) correspond to sequences of phages RB43 and Phi1. Mutations introduced in the loop region (green) correspond to the sequence of phage S-PM2. The F348A mutation was incorporated into all the constructs because it enhanced the solubility of the *E. coli*-expressed Soc-fused recombinant peptides. (C) Effects of swap mutant Soc-HLH peptides on DNA packaging. DNA packaging assays were performed according to the procedure described in Materials and Methods. Proheads (4×10^9 particles) were incubated with increasing concentrations of the mutant peptides (5, 7.5, or 9 μM) for 15 min. The agarose gel shows the amount of DNA packaged in the absence of peptide (lane 1), in the presence of WT peptide (lane 2) or increasing amounts of mutant peptides (lanes 3 to 11). (D) Relative amounts of DNA packaged in the reactions in panel C.

occur in nature. We analyzed one of these sites involved in motor-portal interactions, which provides new insights into the mechanism of ATPase coupling to DNA translocation.

Specificity of portal-motor interactions. Assembly of the packaging motor at the portal vertex must involve interaction with the dodecameric portal (gp20), the 5-fold major capsid protein (gp23*; the star indicates the cleaved form), or both. Our results using a direct binding assay show that gp17 interacts with the portal and proheads lacking the portal are devoid of gp17 binding. This, however, does not rule out gp17 interaction with the major capsid protein because such an interaction might require a primary interaction with the portal. These results are in agreement with the genetic and biochemical data from phages T3, SPP1, and λ (29, 32, 46), as well as our previous genetic data on T4 (25), leading to the conclusion that specific interaction between portal and large terminase is an essential step in the assembly of the phage packaging machine.

Portal binding sites in gp17. In phages T3 and λ, the C-terminal-most 6 to 10 amino acids are implicated in portal binding. The putative interaction sequences, LSGEDE in λ gpA and LYWEDD in T3 gp19, are thought to form hydrophobic and electrostatic interactions (25, 28, 29, 45, 46). Consistent with these observations, nearly all mutations implicated in phage T4 portal interactions occurred at hydrophobic residues. However, phage T4 does not have an analogous portal binding sequence at the C terminus of gp17, but genetic studies and sequence alignments identified two similar sequences, one in the central region of gp17 (site 1; LYNDEDIFDD [aa 323 to 331]) and another in the C-terminal domain (site II; FIDYADKDD [aa 559 to 567]). Although both of these sequences are conserved in T4 family terminases (25, 26), our mutagenesis data showed that only the site I residues (FDD), but not the site II residues (FDY), are critical for function.

The central portal binding site. A packaging-defective mutant of the portal (*cs*N33; D281E-M292I) is suppressed by an Ile-to-Phe *ts* mutation at residue 364 of gp17. In fact, several *ts* mutations are clustered in this central region, all accumulating empty proheads, suggesting a failure to initiate packaging, presumably due to portal interaction defects (25). This region is located in subdomain II, a domain that controls ATP hydrolysis and coupling to DNA translocation. Fitting of the gp17 X-ray structure into the cryo-EM density of the packaging machine, although low resolution (32 Å), indicates that residues in this region might be in contact with the protruding $\alpha\beta$ domain of the portal (Fig. 5). These results combined with the mutational and biochemical analyses (see below) suggest that this central binding site forms, at least in part, the portal interaction site.

The C-terminal portal binding site. A C-terminal *ts* mutation at residue 583 of gp17 (*ts*L51; Ser to Asn) is suppressed by a Met-to-Ile *cs* mutation at residue 308 of gp20, implicating the gp17 C-domain in portal interaction (25). Prohead binding and packaging inhibition studies show that the C-domain also binds to proheads; however, this interaction appears to be nonspecific. Distance measurements between a gfp-labeled gp20 and a fluorescently N- or C-terminus-labeled gp17 put the C terminus of gp17 slightly closer to the portal than the N terminus (9). On the other hand, a gp17 C-terminal truncation mutant lacking the last 33

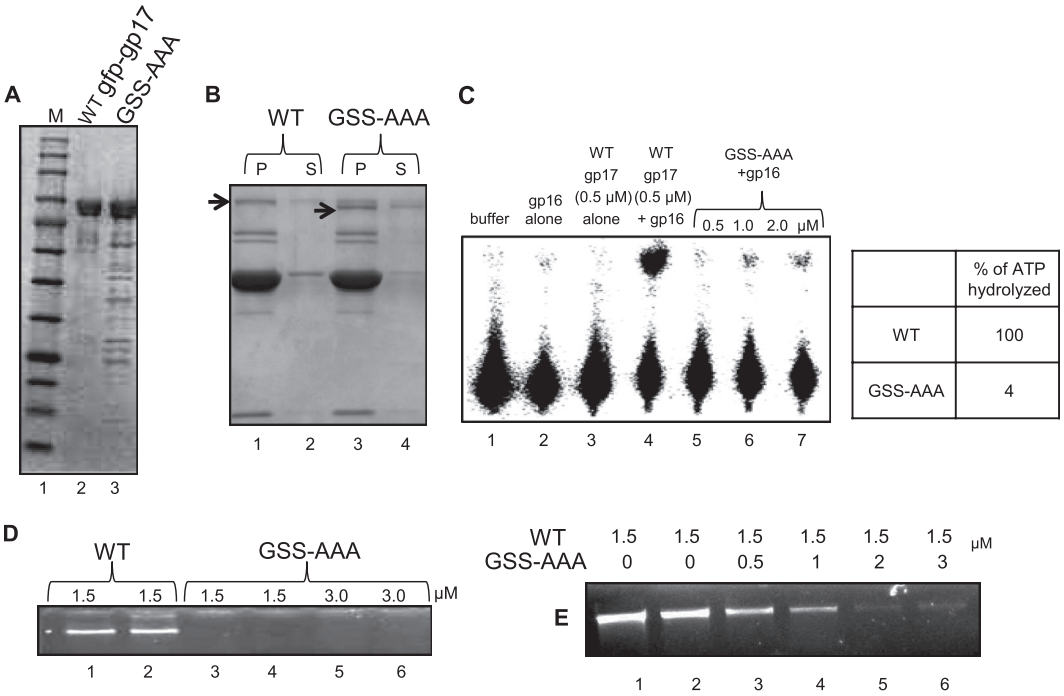

FIG 8 Mutations in the HLH loop do not affect portal binding but lead to loss of DNA packaging. (A) Polyacrylamide gel showing the mobility and purity of WT gfp-gp17 and GSS-AAA gfp-gp17. The lower molecular bands seen are the degradation products of gfp-gp17. (B) The prohead binding assays and *in vitro* DNA packaging assays were performed according to the procedures described in Materials and Methods. Proheads (2×10^{11} particles; lane 1) were incubated with either WT gfp-gp17 (lane 2) or the gfp-gp17 GSS-AAA mutant (lane 4). The unbound gfp-gp17 and gfp-gp17 GSS-AAA proteins present in the supernatant fraction (labeled as "S") are shown in lanes 2 and 4, respectively. The bound gfp-gp17 and gfp-gp17 GSS-AAA proteins present in the pellet (labeled as "P") are shown in lanes 1 and 3, respectively. (C) The gp16-stimulated ATPase activity of WT and GSS-AAA gp17s was determined as described in Materials and Methods. The quantified data are shown in the table. (D) Agarose gel showing the lack of *in vitro* DNA packaging activity in the gfp-gp17 GSS-AAA loop mutant. Proheads (4×10^9 particles) were incubated with 1.5 or 3 μM gfp-gp17 or the gfp-gp17 GSS-AAA mutant for 15 min at room temperature before the rest of the packaging components were added. (E) Packaging inhibition by the GSS-AAA mutant. Proheads (4×10^9 particles) and WT gfp-gp17 were incubated with increasing concentrations of gfp-gp17 GSS-AAA for 15 min before the rest of the packaging components were added. See Materials and Methods for additional details on the DNA packaging assay.

amino acids packages DNA *in vitro* nearly as well as the WT and also retains the ATPase and nuclease activities. These results argue against an essential portal binding site at the C terminus of gp17. Alternatively, the portal interaction surface might involve residues from both the central region as well as the C-terminal domain. The truncated gp17 used for crystallization lacks the last 43 amino acids (aa 567 to 610), and the last 14 amino acids of the structure (aa 553 to 566) are disordered in the crystal structure (41). Therefore, about 57 C-terminal amino acids are missing in the gp17 structure. Thus, if the C terminus were to interact with the central region, it must be in an extended conformation.

HLH motif interacts with the portal. A series of analyses have established that the HLH motif (aa 333 to 353) that is immediately adjacent to the portal binding site I (aa 322 to 331) interacts with the portal. The HLH motif is predicted to be structurally conserved among all the T4 family large terminases, and second site substitutions in this motif compensate for *ts* mutations at portal binding site I. Perhaps the most compelling evidence for a direct interaction between HLH and portal is that an HLH peptide effectively competes with WT gp17 for portal interaction. When both were present in the packaging reaction, the peptide blocked DNA translocation by gp17, presumably by preventing the assembly of a functional motor at the portal. Subtle changes in the helices of HLH reduced binding, whereas mutations in the loop residues did not affect prohead binding. However, mutations in the loop residues resulted in nearly complete loss of ATPase and DNA packaging activities. These results lead to the hypothesis that the HLH helices are important for motor binding to the portal, whereas the loop-portal interactions are important for stimulation of ATP hydrolysis. Consistent with this hypothesis, the predicted secondary structure of HLH is conserved among the T4-related phages, but the amino acid sequences of the helices vary, indicative of their role in conferring specificity to recognize the cognate packaging partner.

Motor-interacting region of the portal protein. Despite lacking significant sequence similarity, the dodecameric portal of tailed phages and herpesviruses is structurally conserved. Where X-ray structural information is available, the cone-shaped portal consists of a wide "crown" inside the capsid, an angular "stem" formed by long helices (two per subunit), and a narrow $\alpha\beta$ domain "stalk" that protrudes outside the capsid (23, 31, 38). Previous genetic and biochemical studies established that the gp17 interaction site resides in the central region of gp20 sequence DR RVWYVDTGNMPARKAAEHMQHVMNTMKNR (aa 281 to 311), and a synthetic peptide corresponding to aa 287 to 300 (underlined) inhibited *in vitro* DNA packaging (25). Indeed, structural modeling of the T4 portal (V. Padilla-Sanchez and V. B. Rao, unpublished data) shows that these gp17-interacting residues are part of the protruding $\alpha\beta$ domain, as was also the case in the X-ray structure of SPP1 portal. These observations lead to another com-

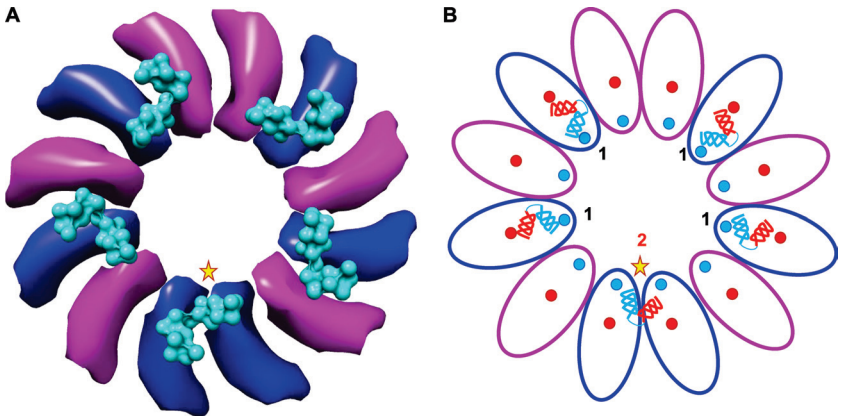

FIG 9 The symmetrically mismatched motor-portal interface contains one unique gp17-gp20 interaction. (**A**) Fitting of the gp17 pentamer (3EZK) into the cryo-EM density of the packaging machine (32 Å; EMDB ID no. 1572) shows that the HLH motif (cyan surface) interacts with the stalk region of dodecameric portal. The gp17-interacting portal subunits are shown in blue, and the noninteracting subunits are shown in magenta (only the HLH and stalk regions are shown). The HLH interactions are of two types: one unique interaction with 2 portal subunits (star) and four nearly equivalent interactions with 1 portal subunit. (B) Schematic illustrating the 2-1-1-1-1 interaction pattern. The HLH motif (illustrated in red and blue helices) interacts with portal loops (shown as red and blue circles). The active subunit (star) also interacts with the same loops, but those of two adjacent portal subunits rather than those of a single subunit (note the positions of the red and blue helices with respect to the red and blue portal loops).

mon theme in that the $\alpha\beta$ domain residues, most likely those in the two structurally conserved loops, interact with the HLH residues that are most proximal to the portal (see the EM fit in Fig. 5).

Communication between portal and motor. In our previously proposed mechanism, the packaging motor exists in two conformational states, relaxed and tensed. ATP binding to the relaxed ATPase domain leads to DNA binding to the C-domain translocation groove. This causes a conformational change that positions the arginine finger into the catalytic center, triggering ATP hydrolysis. The repulsion between the negatively charged products [ADP(3−) and P_i(3−)] drive them apart, causing ATPase subdomain II to rotate by 6°, aligning the charged pairs between the N- and C-domains. This attracts the C-domain-DNA complex, moving it upwards by 7 Å to attain the tensed state and translocate 2 bp of DNA. Product release and loss of negative charges causes subdomain II to rotate back to its original position, misaligning the charged pairs and returning the C-domain to the relaxed state. DNA is then handed over to another subunit, presumably by the matching motor and DNA symmetries. Central to the above mechanism is the coupling of ATP hydrolysis (energy release) to DNA movement (mechanical work). Energy release would not be triggered unless the motor is loaded with both ATP and DNA. The "loaded" state needs to be communicated to the ATPase center through a conformational change, which presumably positions the arginine finger to fire ATP hydrolysis. The ATPase activity of T4 and SPP1 large terminases is stimulated by the portal protein (3, 33), suggesting that this communication step, at least in part, is linked to gp17-portal interactions. This means that the portal-gp17 interaction of the firing ATPase subunit must be different from that of the other portal-gp17 interactions.

Symmetry mismatch between portal and motor. There are two symmetry mismatches in the packaging machine: the well-established mismatch between the five-fold capsid and the dodecameric portal (16) and another between the dodecameric portal and the pentameric packaging motor (27, 41). The symmetry mismatches might impart certain functional or structural advantages to the virus, but what exactly these are remained a mystery. The long-standing notion that the capsid-portal symmetry mismatch provides rotational freedom for the portal, which might drive DNA translocation, has been challenged by recent evidence (4, 18). Our biochemical results combined with structural analyses suggest an alternative view, that the symmetry mismatch provides a mechanistic linkage between ATP hydrolysis and mechanical work.

Symmetry mismatch is expected to impose nonequivalent interactions between the portal and the motor, but nonequivalence is not necessary if as stated, portal interaction with the firing motor subunit is different from those with the other four subunits. In our model, the interacting elements of gp17 are the residues of the two HLH helices, and those of gp20 are the two loops hanging down from the protruding $\alpha\beta$ domain (Fig. 9). If the HLH of the active gp17 (Fig. 9, star) "inserts" between two portal subunits (Fig. 9; see the movie in the supplemental material), then the other four gp17s would be positioned to interact with one portal subunit and would be nearly equivalent, or quasiequivalent, given some flexibility among the subunits. The "unique" gp17 subunit interacts with the same $\alpha\beta$ domain loops as the other four, but from two adjacent portal subunits, whereas the other four interactions are with a single portal subunit, giving a 2-1-1-1-1 pattern (Fig. 9B). For the unique interaction to occur, the HLH (which is part of ATPase subdomain II) must rotate to contact the loop of the adjacent subunit and might also involve "opening up" of some of the helix residues to provide a large interacting surface and binding energy. Indeed, rotation of subdomain II is evident in the crystal structures when gp17 changes conformation from the "relaxed" to "tensed" state (41) (see below).

A molecular lever mechanism for ATPase coupling. Our structural analyses suggest a path by which the unique HLH-portal interaction can be relayed to the arginine finger via a network of hydrogen bonds (Fig. 10). In the relaxed state, shown by a structural model generated by molecular dynamics simulations (Fig. 10A) (14), the S344 residue of the HLH loop is well connected, forming four hydrogen bonds with other HLH residues (ma-

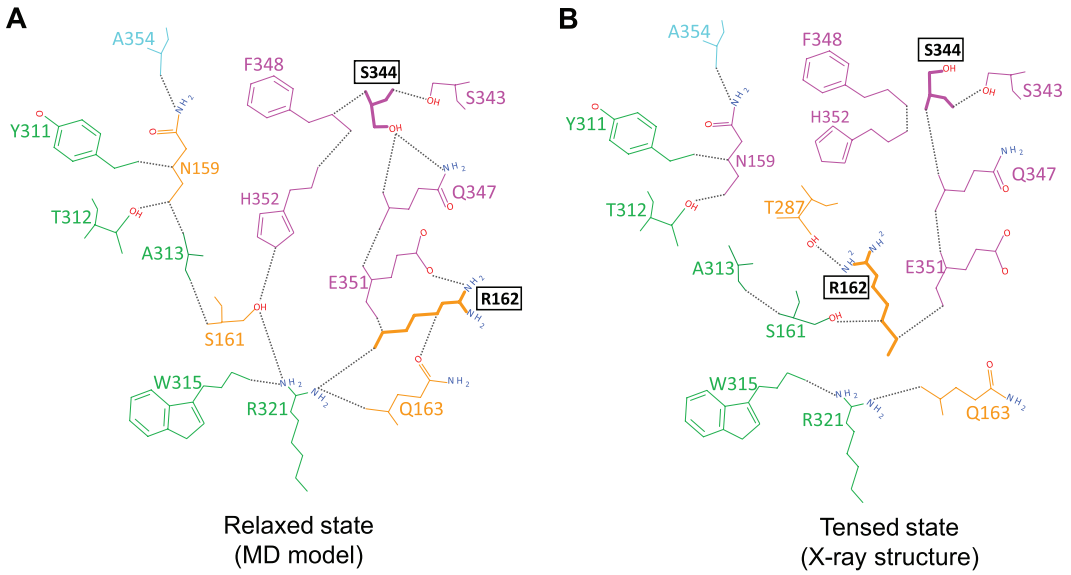

FIG 10 Portal-HLH interaction can signal ATP hydrolysis. (A) The relaxed state of gp17 (model generated from MD simulations) (14) shows a network of hydrogen bonds connecting HLH residues (magenta) to residues of ATPase subdomain I (orange), ATPase subdomain II (green), and the interdomain hinge (cyan). (B) The tensed state of gp17 (PDB ID no. 3CPE) (41) shows a remodeling of the HLH loop, dissolution of several hydrogen bonds, and a new position of the arginine finger residue in the catalytic center.

genta), which in turn contact the arginine finger residue (R162) and other residues of ATPase subdomain I (orange), subdomain II (green), and the flexible hinge (cyan). However, in the tensed state derived from the X-ray crystal structure, the HLH region and the interacting residues are remodeled, with the arginine finger oriented into the catalytic pocket (Fig. 10B). We propose that the unique interaction between the gp17-DNA-ATP complex and two portal subunits might destabilize the network, allowing the arginine finger to move ~60° toward the ATP catalytic center where it hydrogen bonds with the β,γ phosphates of bound ATP as well as the ATPase coupling residue, T287 (Fig. 10B). This leads to cleavage of the β,γ phosphoanhydride bond followed by P_i capture by T287. Thus, a "distant" interaction between the portal and gp17 HLH might be communicated to the ATPase center through the hydrogen bond network.

The above analyses lead to a "molecular lever" mechanism in which the HLH acts as a lever coupling ATP hydrolysis to DNA movement (see the movie in the supplemental material). Binding of DNA to the translocation groove causes a conformational change in subdomain II leading to the interaction of the lever with two portal subunits (Fig. 9). This unique interaction orients the arginine finger to trigger ATP hydrolysis. The 6° rotation of subdomain II following hydrolysis moves the lever by 5.3 Å to insert between the portal subunits, stabilizing this transient state. A tensed state is thus achieved, translocating the bound DNA. Product release relieves the torsional stress of subdomain II, destabilizing the HLH-portal interaction and returning the motor and portal subunits to the relaxed state. When the DNA is handed over to the next motor subunit, this cycle repeats by inserting the lever once again into the portal subunits and firing that ATPase subunit. The unique lever interactions "travel" through the packaging machine subunits, ensuring ATPase firing only when the motor is loaded with both ATP and DNA (see the movie in the supplemental material).

In conclusion, a series of observations are consistent with the molecular lever mechanism: HLH-portal interactions connecting the portal and the regulatory ATPase subdomain II, structural analyses linking HLH to the arginine finger, 6° rotation of subdomain II during conformational transition, and symmetry mismatch creating one unique portal-motor interaction. Further mutational and structural analyses would be necessary to determine if such a central role for the portal is justified as well as elucidate additional molecular details of the coupling mechanism.

ACKNOWLEDGMENTS

We thank Michael Rossmann and Siyang Sun (Purdue University), Michael Feiss (University of Iowa College of Medicine), and Lindsay Black (University of Maryland, College Park) for critical reviews of the manuscript and for thoughtful comments and Tanfis I. Alam (The Catholic University of America) for help with experiments shown in Fig. 8.

This work was supported by grants from the National Science Foundation (MCB-0923873) and the National Institute of Allergy and Infectious Diseases (R01AI081726).

The authors declare that they have no conflicts of interest.

REFERENCES

1. **Alam TI, et al.** 2008. The headful packaging nuclease of bacteriophage T4. Mol. Microbiol. **69**:1180–1190.
2. **Al-Zahrani AS, et al.** 2009. The small terminase, gp16, of bacteriophage T4 is a regulator of the DNA packaging motor. J. Biol. Chem. **284**:24490–24500.
3. **Baumann RG, Black LW.** 2003. Isolation and characterization of T4 bacteriophage gp17 terminase, a large subunit multimer with enhanced ATPase activity. J. Biol. Chem. **278**:4618–4627.
4. **Baumann RG, Mullaney J, Black LW.** 2006. Portal fusion protein constraints on function in DNA packaging of bacteriophage T4. Mol. Microbiol. **61**:16–32.
5. **Black LW, Peng G.** 2006. Mechanistic coupling of bacteriophage T4 DNA packaging to components of the replication-dependent late transcription machinery. J. Biol. Chem. **281**:5635–25643.
6. **Buttner CR, et al.** 2012. Structural basis for DNA recognition and loading into a viral packaging motor. Proc. Natl. Acad. Sci. U. S. A. **109**:811–816.
7. Reference deleted.
8. **Casjens SR, et al.** 1992. Bacteriophage P22 portal protein is part of the

gauge that regulates packing density of intravirion DNA. J. Mol. Biol. **224**:1055–1074.
9. **Dixit A, Ray K, Lakowicz JR, Black LW.** 2011. Dynamics of the T4 bacteriophage DNA packasome motor: endonuclease vii resolvase release of arrested Y-DNA substrates. J. Biol. Chem. **286**:18878–18889.
10. **Fang H, Jing P, Haque F, Guo P.** 2012. Role of channel lysines and the "push through a one-way valve" mechanism of the viral DNA packaging motor. Biophys. J. **102**:127–135.
11. **Frackman S, Siegele DA, Feiss M.** 1985. The terminase of bacteriophage lambda. Functional domains for *cos*B binding and multimer assembly. J. Mol. Biol. **183**:225–238.
12. **Fuller DN, Raymer DM, Kottadiel VI, Rao VB, Smith DE.** 2007. Single phage T4 DNA packaging motors exhibit large force generation, high velocity, and dynamic variability. Proc. Natl. Acad. Sci. U. S. A. **104**:16868–16873.
13. **Gao S, Rao VB.** 2011. Specificity of interactions among the DNA-packaging machine components of T4-related bacteriophages. J. Biol. Chem. **286**:3944–3956.
14. **Ghosh-Kumar M, Alam TI, Draper B, Stack JD, Rao VB.** 2011. Regulation by interdomain communication of a headful packaging nuclease from bacteriophage T4. Nucleic Acids Res. **39**:2742–2755.
15. **Goetzinger KR, Rao VB.** 2003. Defining the ATPase center of bacteriophage T4 DNA packaging machine: requirement for a catalytic glutamate residue in the large terminase protein gp17. J. Mol. Biol. **331**:139–154.
16. **Hendrix RW.** 1978. Symmetry mismatch and DNA packaging in large bacteriophages. Proc. Natl. Acad. Sci. U. S. A. **75**:4779–4783.
17. **Horton RM, Cai ZL, Ho SN, Pease LR.** 1990. Gene splicing by overlap extension: tailor-made genes using the polymerase chain reaction. Biotechniques **5**:528–535.
18. **Hugel T, et al.** 2007. Experimental test of connector rotation during DNA packaging into bacteriophage ϕ29 capsids. PLoS Biol. **5**:e59. doi:10.1371/journal.pbio.0050059.
19. **Kanamaru S, Kondabagil K, Rossmann MG, Rao VB.** 2004. The functional domains of bacteriophage T4 terminase. J. Biol. Chem. **279**:40795–40801.
20. **Kondabagil K, Zhang Z, Rao VB.** 2006. The DNA translocating ATPase of bacteriophage T4 packaging motor. J. Mol. Biol. **363**:786–799.
21. **Kuebler D, Rao VB.** 1998. Functional analysis of the DNA-packaging/terminase protein gp17 from bacteriophage T4. J. Mol. Biol. **281**:803–814.
22. **Lander GC, et al.** 2006. The structure of an infectious P22 virion shows the signal for headful DNA packaging. Science **312**:1791–1795.
23. **Lebedev AA, et al.** 2007. Structural framework for DNA translocation via the viral portal protein. EMBO J. **26**:1984–1994.
24. **Leffers G, Rao VB.** 2000. Biochemical characterization of an ATPase activity associated with the large packaging subunit gp17 from bacteriophage T4. J. Biol. Chem. **275**:37127–37136.
25. **Lin H, Rao VB, Black LW.** 1999. Analysis of capsid portal protein and terminase functional domains: interaction sites required for DNA packaging in bacteriophage T4. J. Mol. Biol. **289**:249–260.
26. **Mitchell MS, Matsuzaki S, Imai S, Rao VB.** 2002. Sequence analysis of bacteriophage T4 DNA packaging/terminase genes 16 and 17 reveals a common ATPase center in the large subunit of viral terminases. Nucleic Acids Res. **30**:4009–4021.
27. **Morais MC, et al.** 2008. Defining molecular and domain boundaries in the bacteriophage phi29 DNA packaging motor. Structure **16**:1267–1274.
28. **Morita M, Tasaka M, Fujisawa H.** 1995. Analysis of the fine structure of the prohead binding domain of the packaging protein of T3 using a hexapeptide, an analog of prohead binding site. Virology **211**:516–524.
29. **Morita M, Tasaka M, Fujisawa H.** 1995. Structural and functional domains of the large subunit of the bacteriophage T3 DNA packaging enzyme: importance of the C-terminal region in prohead binding. J. Mol. Biol. **245**:635–644.
30. **Nemecek D, Lander GC, Johnson JE, Casjens SR, Thomas GJ, Jr.** 2008. Assembly architecture and DNA binding of the bacteriophage P22 terminase small subunit. J. Mol. Biol. **383**:494–501.
31. **Olia AS, Prevelige PE, Johnson JE, Cingolani G.** 2011. Three-dimensional structure of a viral genome-delivery portal complex. Nat. Struct. Mol. Biol. **18**:597–603.
32. **Oliveira L, Henriques AO, Tavares P.** 2006. Modulation of the viral ATPase activity by the portal protein correlates with DNA packaging efficiency. J. Biol. Chem. **281**:21914–21923.
33. **Oliveira L, Cuervo A, Tavares P.** 2010. Direct interaction of the bacteriophage SPP1 packaging ATPase with the portal protein. J. Biol. Chem. **285**:7366–7373.
34. **Qin L, Fokine A, O'Donnell E, Rao VB, Rossmann MG.** 2010. Structure of the small outer capsid protein, Soc: a clamp for stabilizing capsids of T4-like phages. J. Mol. Biol. **395**:728–741.
35. **Rao VB, Feiss M.** 2008. The bacteriophage DNA packaging motor. Annu. Rev. Genet. **42**:647–681.
36. **Rao VB, Black LW.** 2005. DNA packaging in bacteriophage T4, p 40–58. *In* C. Catalano (ed), Viral genome packaging machines: genetics, structure and mechanism. Landes Biosciences, Georgetown, TX.
37. **Roy A, Bhardwaj A, Cingolani G.** 2011. Crystallization of the nonameric small terminase subunit of bacteriophage P22. Acta Crystallogr. Sect. F Struct. Biol. Cryst. Commun. **67**:104–110.
38. **Simpson AA, et al.** 2000. Structure of the bacteriophage phi29 DNA packaging motor. Nature **408**:745–750.
39. **Smith DE, et al.** 2001. The bacteriophage straight phi29 portal motor can package DNA against a large internal force. Nature **413**:748–752.
40. **Sun S, et al.** 2012. Structure and function of the small terminase component of the DNA packaging machine in T4-like bacteriophages. Proc. Natl. Acad. Sci. U. S. A. **109**:817–822.
41. **Sun S, et al.** 2008. The structure of the phage T4 DNA packaging motor suggests a mechanism dependent on electrostatic forces. Cell **135**:1251–1262.
42. **Sun S, Kondabagil K, Gentz PM, Rossmann MG, Rao VB.** 2007. The structure of the ATPase that powers DNA packaging into bacteriophage T4 procapsids. Mol. Cell **25**:943–949.
43. **Tavares P, et al.** 1992. Identification of a gene in Bacillus subtilis bacteriophage SPP1 determining the amount of packaged DNA. J. Mol. Biol. **225**:81–92.
44. **Tsien RY.** 1998. The green fluorescent protein. Annu. Rev. Biochem. **67**:509–544.
45. **Yeo A, Feiss M.** 1995. Mutational analysis of the prohead binding domain of the large subunit of terminase, the bacteriophage lambda DNA packaging enzyme. J. Mol. Biol. **245**:126–140.
46. **Yeo A, Feiss M.** 1995. Specific interaction of the terminase, the DNA packaging enzyme of bacteriophage lambda, with the portal protein of the prohead. J. Mol. Biol. **245**:141–150.
47. **Zhao H, et al.** 2010. Crystal structure of the DNA-recognition component of the bacterial virus Sf6 genome-packaging machine. Proc. Natl. Acad. Sci. U. S. A. **107**:1971–1976.